

Study on the Dynamics of Phase Formation and Degradation of 2D Layered Hybrid Perovskites and Low-dimensional Hybrids Containing Mono-functionalized Oligothiophene Cations

Peer-reviewed author version

VAN GOMPEL, Wouter; HERCKENS, Roald; MERTENS, Martijn; DENIS, Paul-Henry; RUTTENS, Bart; D'HAEN, Jan; Van Hecke, K; LUTSEN, Laurence & VANDERZANDE, Dirk (2021) Study on the Dynamics of Phase Formation and Degradation of 2D Layered Hybrid Perovskites and Low-dimensional Hybrids Containing Mono-functionalized Oligothiophene Cations. In: ChemNanoMat, 7 (9) , p. 1013 -1019.

DOI: 10.1002/cnma.202100169

Handle: <http://hdl.handle.net/1942/36149>

# Study on the dynamics of phase formation and degradation of 2D layered hybrid perovskites and low-dimensional hybrids containing mono-functionalized oligothiophene cations

Wouter T.M. Van Gompel,<sup>[a]†</sup> Roald Herckens,<sup>[a]†</sup> Martijn Mertens,<sup>[a]</sup> Paul-Henry Denis,<sup>[a]</sup> Bart Ruttens,<sup>[b]</sup> Jan D'Haen,<sup>[b]</sup> Kristof Van Hecke,<sup>[c]</sup> Laurence Lutsen,<sup>[b]</sup> and Dirk Vanderzande<sup>\*[a][b]</sup>

[a] Dr. W.T.M. Van Gompel, Dr. R. Herckens, M. Mertens, P.-H. Denis, Prof. Dr. D. Vanderzande  
Hybrid Materials Design (HyMaD), Institute for Materials Research (IMO-IMOMECE)  
Hasselt University

Martelarenlaan 42, B-3500 Hasselt, Belgium  
E-mail: dirk.vanderzande@uhasselt.be

[b] B. Ruttens, Prof. Dr. J. D'Haen, Dr. L. Lutsen, Prof. Dr. D. Vanderzande  
Associated Laboratory IMOMECE  
Imec

Wetenschapspark 1, B-3590 Diepenbeek, Belgium

[c] Prof. Dr. K. Van Hecke  
XStruct, Department of Chemistry  
Ghent University

Krijgslaan 281-S3, B-9000 Ghent, Belgium

Supporting information for this article is given via a link at the end of the document.

**Abstract:** Low-dimensional (2D or 1D) hybrid perovskites are receiving increased attention due to their structural flexibility and enhanced stability compared to their 3D counterparts. Understanding the phase formation and degradation behavior of these materials is crucial towards their use in optoelectronic devices, since different crystal phases possess different optical and electronic properties. In this communication, we study the phase formation and degradation of a series of hybrids containing bithiophene, terthiophene and quaterthiophene derivatives. We show that two crystal phases can be formed for each of these systems, depending on the processing conditions. One phase corresponds to a 2D layered perovskite and the other phase has optical properties corresponding to a dimensionality intermediate between a 2D and a 1D hybrid.

Hybrid organic-inorganic perovskites have received a lot of research attention over the past years, mainly due to their use as active materials in solar cells. Next to the interest in 3D hybrid perovskites, which are employed primarily in solar cells, interest in 0D, 1D, 2D, and multi-layered hybrid perovskites is growing. These lower-dimensional hybrids have envisaged applications including solar cells, light-emitting diodes, photodetectors and transistors.<sup>[1]</sup> Advantages of these lower-dimensional materials compared to their 3D counterparts include a generally enhanced material stability<sup>[1a, 1c, 2]</sup>, and a much higher tolerance towards the size of the organic cation that can be incorporated into the structure<sup>[1a, 3]</sup>. Due to this high structural flexibility, the use of larger, functional, organic cations becomes viable.<sup>[1a-c]</sup> Such functional organic cations can, for example, impart specific absorption<sup>[4]</sup>, emission<sup>[5]</sup>, or charge transfer<sup>[6]</sup> characteristics to the hybrid. Besides a potential direct effect of the organic cations on the electronic properties, the distortion of the inorganic lattice induced by the stacking of the molecules in the organic layer also influences the absorption and emission characteristics of the hybrid.<sup>[5b, 7]</sup>

Depending on the characteristics of the applied organic cation, as well as the conditions present during crystallization, hybrids of different dimensionalities can be obtained.<sup>[3a, 6d, 8]</sup> The structural dimensionality (corresponding to the connectivity of the  $\text{PbI}_6^{4-}$  octahedra) can be 3D, 2D, 1D, or 0D. Next to a structural dimensionality, also an electronic dimensionality can be defined.<sup>[9]</sup> The electronic dimensionality of a material is described as the connectivity of the atomic-orbitals that comprise the lower conduction band and upper valence band for the compound. The

electronic dimensionality can be lower than the structural dimensionality and this influences the optical and electronic properties of the material.<sup>[9-10]</sup> In this regard, Kamminga et al. showed that the presence of face- or edge-sharing octahedra next to corner-sharing octahedra in a hybrid structure results in a wider bandgap and effectively a reduced electronic dimensionality.<sup>[11]</sup>

Oligothiophenes have been studied extensively as organic semiconductors for use in applications such as organic light-emitting diodes (OLEDs) and organic field-effect transistors (OFETs).<sup>[12]</sup> The incorporation of an oligothiophene into the organic layer of a 2D hybrid perovskite was first described by D.B. Mitzi et al.<sup>[13]</sup>, who introduced a quaterthiophene derivative functionalized with two alkylammonium chains. In 2003, Zhu et al.<sup>[14]</sup> compared the influence of a mono- and a di-ammonium cation of 2,2'-bithiophene on the formation of hybrid crystals. Recently, the use of oligothiophenes in the organic layer of a 2D perovskite has received significant attention again from a theoretical and experimental point of view.<sup>[15]</sup> It was shown that by tuning the number of thiophene units in these oligothiophenes, as well as the halide of the inorganic framework, different types of internal quantum well alignment can be obtained.<sup>[15a, 15b]</sup> Next to this, efficient separation of charges between the organic oligothiophene layer and the inorganic layer was demonstrated, resulting in a long-lived charge-separated state.<sup>[15c, 15d]</sup> However, less attention has been devoted to elucidating the details of the phase formation and degradation behavior of such oligothiophene-containing 2D layered perovskites.

We apply a mono-alkylammonium quaterthiophene derivative as a model system for a detailed study of the phase formation and degradation in thin films and compare this model system to the hybrids containing mono-alkylammonium oligothiophenes with less thiophene units. We find that the different mono-alkylammonium oligothiophenes behave very similarly in that they can give rise to two types of crystal phases, depending on the processing conditions. Comparing the excitonic absorption peak positions of the obtained oligothiophene-containing hybrids to those of previously synthesized hybrids, we can assign one of these phases to a 2D layered perovskite. In contrast, the other phase is assigned a lower electronic dimensionality in between that of 2D layered perovskites and 1D hybrids.

A mono-functionalized quaterthiophene derivative with a propylammonium chain was synthesized (Figure 1). A precursor solution with a stoichiometry of  $A_2PbI_4$  (A being this derivative) was prepared in dry DMF.

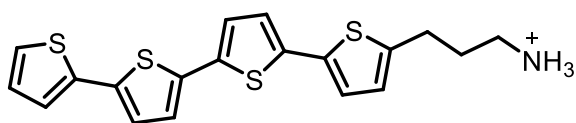


**Figure 1.** Structure of the quaterthiophene derivative (Quat-C<sub>3</sub>).

The precursor solution was spin-coated onto quartz substrates, and the resulting thin films were annealed on a hotplate inside a glovebox. The first notable characteristic is the relatively high annealing temperature required for the formation of the hybrid phase, based on the appearance of the excitonic peak at ~ 444 nm (2.79 eV) (Figure 2). Annealing at 110 °C for 15 min does not result in the formation of the hybrid structure, as the bandgap of the precursor lead iodide can be discerned in the absorption spectrum of the film. At progressively higher annealing temperatures, the intensity of the excitonic absorption peak at 444 nm increases, indicative of the more extensive structure formation. For hybrids containing small flexible molecules such as butylammonium or phenethylammonium, the annealing temperature needed is generally much lower. In fact, both  $(BA)_2PbI_4$  (BA = butylammonium) as well as  $(PEA)_2PbI_4$  (PEA = phenethylammonium) can be formed in thin films without annealing.<sup>[16]</sup> Mitzi *et al.* employed a high annealing temperature of 200 °C for 30 min for a film containing a quaterthiophene derivative functionalized with one alkylammonium chain at each side, although it must be noted that they used a single source thermal ablation method to deposit the films instead of spin-coating.<sup>[13a]</sup> The X-ray diffraction pattern of a spin-coated film of  $(Quat-C_3)_2PbI_4$  annealed at 200 °C is shown in Figure 3. The pattern consists of equally-spaced reflections, with a calculated *d*-spacing of ~ 27.7 Å. For comparison, the length of a single Quat-C<sub>3</sub> molecule is ~ 19.7 Å. This hybrid with an excitonic absorption peak at ~ 444 nm, obtained *via* spin-coating, will be abbreviated as  $(Quat-C_3)_2PbI_4$ -SC from now on.

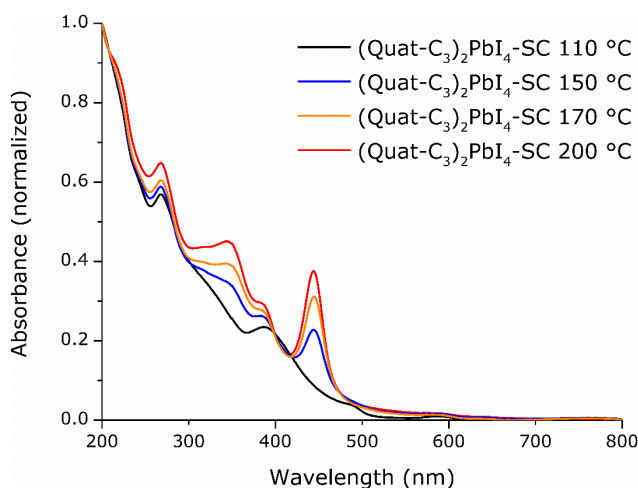


**Figure 2.** Absorption spectra of films of  $(Quat-C_3)_2PbI_4$ -SC, annealed at different temperatures for 15 min.

Remarkably, we find that using an alternative processing method, namely drop-casting, consistently results in the formation of a different hybrid when starting from an identical precursor solution with the same stoichiometry. When the precursor solution of  $(Quat-C_3)_2PbI_4$  is drop-casted onto a quartz substrate, a hybrid with an excitonic absorption peak located at ~ 505 nm (2.46 eV)

is obtained after annealing (Figure 4). The XRD pattern of this film consists of equally spaced reflections similar to the pattern of  $(Quat-C_3)_2PbI_4$ -SC but shifted to higher diffraction angles indicating a reduced *d*-spacing (~ 24.7 Å) compared to  $(Quat-C_3)_2PbI_4$ -SC (Figure 3). The hybrid with an excitonic absorption peak at ~ 505 nm, obtained *via* drop-casting, will be abbreviated as  $(Quat-C_3)_2PbI_4$ -DC hereafter.

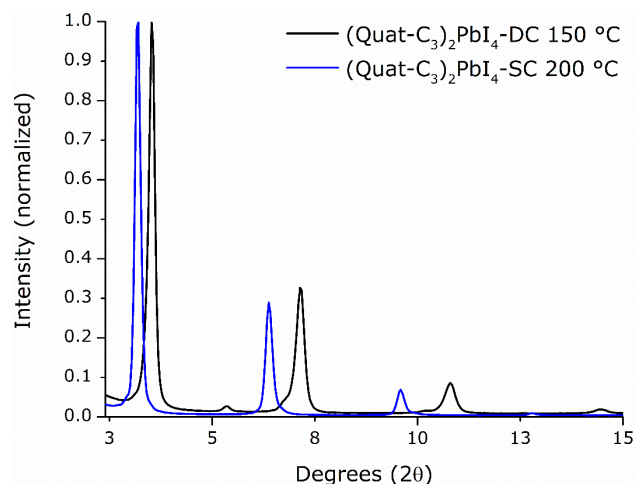


**Figure 3.** Comparison between the X-ray diffraction patterns of a film of  $(Quat-C_3)_2PbI_4$ -DC annealed at 150 °C for 15 min (black) and a film of  $(Quat-C_3)_2PbI_4$ -SC annealed at 200 °C for 15 min (blue).

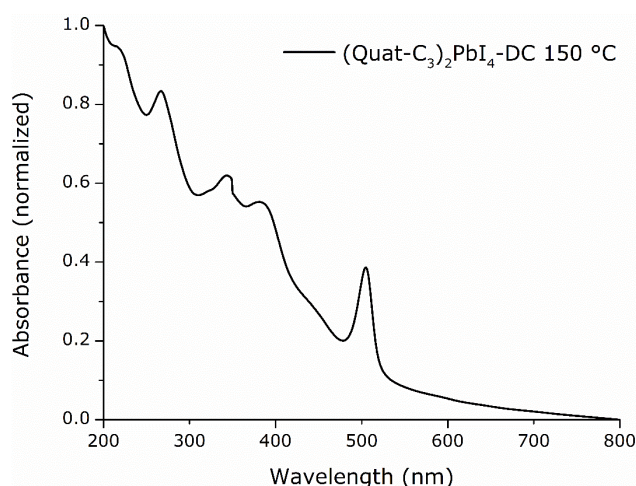


**Figure 4.** The absorption spectrum of a film of  $(Quat-C_3)_2PbI_4$ -DC, annealed at 150 °C for 30 min.

Given that both phases can be obtained from the same precursor solution, using different processing methods, we were interested in the possibility of converting one phase into the other. For this purpose, we carried out *in-situ* temperature-controlled absorption spectroscopy and temperature-controlled X-ray diffraction measurements on films starting from both phases. For the first set of experiments, the precursor solution was drop-casted and the resulting film was dried at 50 °C for 5 min before the start of the *in-situ* heating experiment. Starting from a drop-casted film, the  $(Quat-C_3)_2PbI_4$ -DC phase is initially formed as expected based on the *ex-situ* experiments. As can be seen in Figure 5, this phase can be converted into the  $(Quat-C_3)_2PbI_4$ -SC phase under the influence of temperature. Between 24 °C and 128 °C, the  $(Quat-C_3)_2PbI_4$ -DC phase is present, as evinced by the excitonic peak at ~ 500 nm. Between 150 °C and 196 °C, the  $(Quat-C_3)_2PbI_4$ -SC phase is present, as evinced by the presence of the excitonic peak at ~ 445 nm. At higher temperatures, the SC phase degrades. The conversion from the DC to the SC phase is further exemplified by examining a plot of the absorbance at the wavelengths of the excitonic peaks (~ 445 nm and ~ 500 nm) of

both phases as a function of temperature. A plot of the cross-sections shows that the two lines intersect at  $\sim 122^\circ\text{C}$  (Figure 6). Moreover, there is a clear isosbestic point in the absorption spectra, located at  $\sim 472\text{ nm}$ , during the conversion from one phase into the other (Figure 7). Note that the excitonic peak position of both phases shifts slightly ( $\pm 5\text{ nm}$ ) as a function of temperature. For the cross-sections an average value was chosen.

The  $(\text{Quat-C}_3)_2\text{PbI}_4\text{-DC}$  phase was clearly already formed, based on the presence of the excitonic peak, from a precursor film that was dried at  $50^\circ\text{C}$  (Figure 5). This is in contrast with the high annealing temperature necessary to form  $(\text{Quat-C}_3)_2\text{PbI}_4\text{-SC}$ , starting from a spin-coated film (Figure 2).  $\text{Quat-C}_3$  is a relatively large organic molecule and is likely hard to reorganize to fit into the perovskite structure. We, therefore, hypothesize that the presence of a significantly larger amount of solvent during the crystallization when using the drop-casting approach instead of spin-coating, may impart sufficient mobility to the precursor components such that the required annealing temperature is relatively lowered. This is analogous to the use of "solvent vapor annealing" where films are annealed on a hotplate in an environment deliberately containing a solvent vapor. We have shown earlier that this leads to a lowering of the required annealing temperature for a 2D layered perovskite containing a benzothienobenzothiophene derivative.<sup>[8c]</sup>

Temperature-controlled XRD patterns (Figures S9-S11) conform to the temperature-controlled absorption spectra. The phase with the smaller  $d$ -spacing (corresponding to  $(\text{Quat-C}_3)_2\text{PbI}_4\text{-DC}$ ) transitions into the phase with larger  $d$ -spacing (corresponding to  $(\text{Quat-C}_3)_2\text{PbI}_4\text{-SC}$ ) between  $150^\circ\text{C}$  and  $170^\circ\text{C}$  (Figure S11). This is followed by the degradation of  $(\text{Quat-C}_3)_2\text{PbI}_4\text{-SC}$  into lead iodide (with the main reflection at  $\sim 12.6^\circ 2\theta$ )<sup>[17]</sup>. Note that the exact temperature at which the transition from one phase into the other occurs differs between the two *in-situ* techniques, at  $\sim 160^\circ\text{C}$  for *in-situ* XRD instead or at  $\sim 122^\circ\text{C}$  for *in-situ* UV-Vis. This can be explained by the difference in the measurement of the temperature. In the *in-situ* absorption spectroscopy setup, a thermocouple touches the film, while in the *in-situ* XRD setup, the temperature of the heating chamber is measured instead.

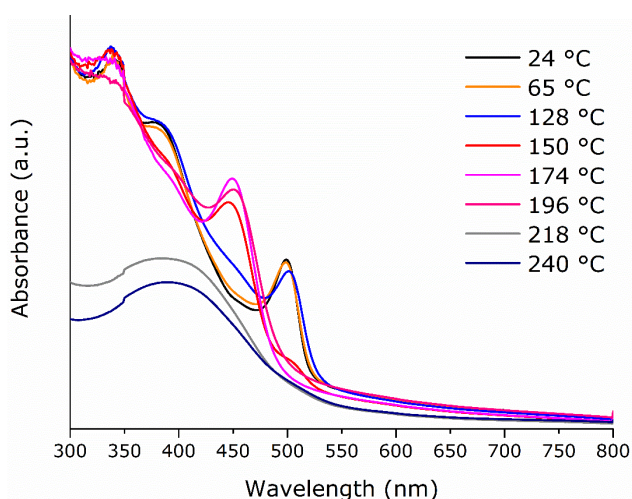


**Figure 5.** Selected absorption spectra as a function of temperature starting from a drop-casted film of  $(\text{Quat-C}_3)_2\text{PbI}_4$  that was dried at  $50^\circ\text{C}$  for 5 min before the *in-situ* experiment.

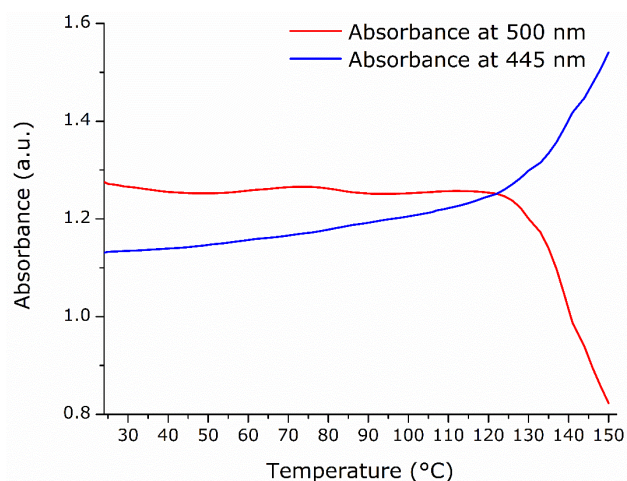


**Figure 6.** Absorbance at 500 nm (red) and at 445 nm (blue) as a function of temperature, extracted from the absorption spectra at different temperatures starting from a drop-casted film of  $(\text{Quat-C}_3)_2\text{PbI}_4$  that was dried at  $50^\circ\text{C}$  for 5 min before the *in-situ* experiment.

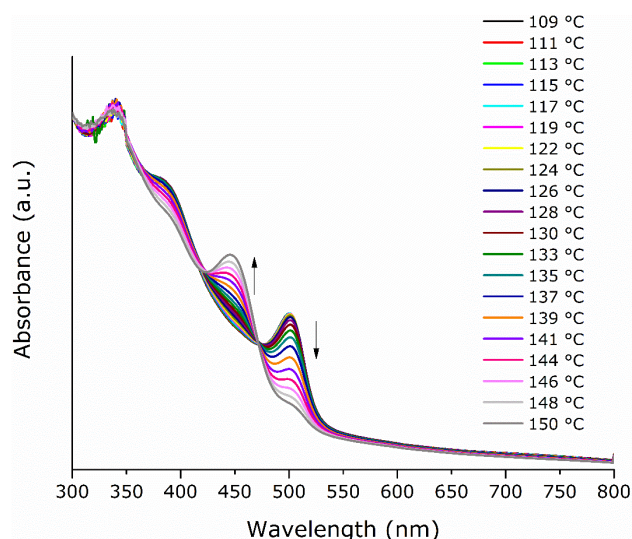


**Figure 7.** Absorption spectra as a function of temperature, between  $109^\circ\text{C}$  and  $150^\circ\text{C}$ , starting from a drop-casted film of  $(\text{Quat-C}_3)_2\text{PbI}_4$  dried at  $50^\circ\text{C}$  for 5 min before the *in-situ* experiment. The black arrows indicate decreasing or increasing absorbance as a function of temperature. This plot uses the data from the same experiment as Figure 6 and 7.

In a second set of experiments, the *in-situ* measurements are started from a spin-coated film previously dried at  $50^\circ\text{C}$  (Figures S12-S16). In this way,  $(\text{Quat-C}_3)_2\text{PbI}_4\text{-SC}$  is formed, as expected, based upon the *ex-situ* experiments. In the absorption spectra, an excitonic peak at  $\sim 449\text{ nm}$  appears between  $108^\circ\text{C}$  and  $150^\circ\text{C}$  and this excitonic peak decreases in intensity between  $152^\circ\text{C}$  and  $194^\circ\text{C}$  (Figure S14). In the XRD patterns, reflections with a  $d$ -spacing of  $27.7\text{ \AA}$  are present and they sharply increase in intensity between  $90^\circ\text{C}$  and  $170^\circ\text{C}$ , followed by a decrease in intensity and concomitant formation of lead iodide, indicative of degradation. Based on these experiments, the  $(\text{Quat-C}_3)_2\text{PbI}_4\text{-SC}$  phase does not transition into a different hybrid phase as a function of temperature but instead degrades directly into lead iodide.

In order to assess the generality of such phase formation behavior for the mono-functionalized oligothiophenes, the terthiophene and bithiophene derivatives were also synthesized, abbreviated as respectively Tert-C<sub>3</sub> and Bit-C<sub>3</sub> (Figure 8).

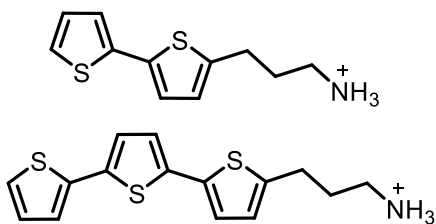


**Figure 8.** Structure of bithiophene (Bit-C<sub>3</sub>; top) and terthiophene (Tert-C<sub>3</sub>; bottom) derivatives.

Using both of these oligothiophene derivatives, two hybrid phases similar to those obtained with Quat-C<sub>3</sub> can be formed, one phase with an excitonic peak in the region around 440 nm (labeled phase 2 from now on) and the other phase with an excitonic peak in the region around 500 nm (labeled phase 1 from now on) (Figure 9). For these shorter oligothiophenes, the conditions for the formation of these two phases do, however, differ from those containing Quat-C<sub>3</sub>. While phase 1 with Quat-C<sub>3</sub> could only be obtained using drop-casting (*vide supra*), this is not the case for the shorter oligothiophenes. For both Tert-C<sub>3</sub> as well as Bit-C<sub>3</sub>, the two phases can readily be obtained *via* spin-coating (see Figures S17-S18 for absorption spectra of spin-coated films annealed at different temperatures and Figures S19-S20 for X-ray diffraction patterns of phase 1 and phase 2 of Tert-C<sub>3</sub> and Bit-C<sub>3</sub>). For Tert-C<sub>3</sub>, the phase that is obtained depends on the annealing temperature that is used (phase 2 is obtained at higher annealing temperatures than phase 1, analogous to the corresponding Quat-C<sub>3</sub> phases in the *in-situ* experiments). For Bit-C<sub>3</sub> it was not possible to obtain the two phases separately, they are both present in the films regardless of the annealing temperature that is used (Figure S18). As the number of thiophene units in the oligothiophene decreases, it is clear that the difference in formation behavior between phase 1 and phase 2 decreases, in other words the tendency for one phase to form over the other is reduced. We hypothesize that this is related to the Van der Waals interactions between the oligothiophene molecules in the organic layer that become progressively weaker when the number of thiophene units decreases, resulting in a smaller difference in formation energy between the two phases.

Since the *d*-spacing in the XRD patterns differs significantly between both phases (e.g. 24.7 Å vs. 27.7 Å for the Quat-C<sub>3</sub> hybrids), it is expected that the ordering of the oligothiophenes in the organic layer also differs significantly between both types of hybrid, which is in turn expected to impact the configuration of the inorganic network (e.g. the Pb-I-Pb angles and the connectivity of the octahedra) that is responsible for the excitonic absorption peak position.

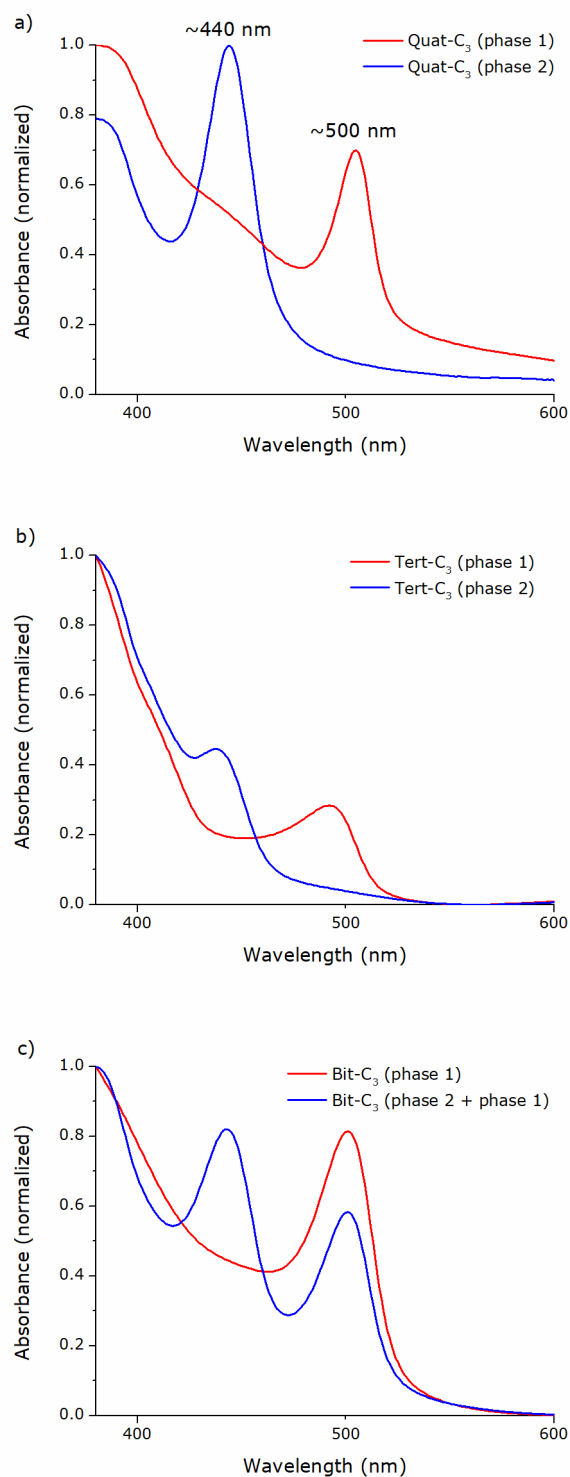


**Figure 9.** Excitonic absorption peaks of the two phases for a) Quat-C<sub>3</sub>, b) Tert-C<sub>3</sub>, and c) Bit-C<sub>3</sub> (phase 1 = red; phase 2 = blue; for Bit-C<sub>3</sub> both phases are present). For Quat-C<sub>3</sub>, the blue curve was obtained from a spin-coated film annealed at 170 °C for 15 min and the red curve from a drop-casted film annealed at 150 °C for 30 min. For Tert-C<sub>3</sub>, the blue and red curves were obtained from spin-coated films annealed at respectively 170 °C and 110 °C for 15 min. For Bit-C<sub>3</sub>, the blue and red curves were obtained from spin-coated films annealed at respectively 170 °C and 150 °C for 15 min.

For phase 2 of these oligothiophene-based hybrids, a wavelength for the excitonic peak of  $\sim 440$  nm is observed, which is relatively far removed from the excitonic absorption peak position of 2D layered perovskites such as  $(\text{BA})_2\text{PbI}_4$  (at  $\sim 510$  nm)<sup>[18]</sup> and  $(\text{PEA})_2\text{PbI}_4$  (at  $\sim 517$  nm)<sup>[19]</sup>. Phase 1 of the oligothiophene series does have an excitonic absorption peak located at  $\sim 500$  nm, which is in the expected wavelength range for 2D layered perovskites. In order to get a better view of the spread in excitonic absorption peak positions that can exist for different types of hybrids with different dimensionalities, we have assembled the excitonic absorption peak positions for a variety of hybrids containing different organic cations from our earlier work as well as from the literature (Figure 10). The absorption spectra with the excitonic absorption peaks of thin films of the hybrids that we synthesized ourselves are shown in Figures S21-S28 of the SI. Note that the excitonic absorption peak position for our prepared reference 2D layered perovskite film,  $(\text{PEA})_2\text{PbI}_4$  (517 nm), matches exactly with a reported value of 2.40 eV (517 nm) in literature<sup>[19]</sup>.

The hybrids with an excitonic peak around 410 nm possess a 1D electronic dimensionality.<sup>[9a]</sup>  $(\text{Apy-C}_2)\text{PbI}_3$  and  $(\text{piper})\text{PbI}_3$  have been shown to be structurally 1D hybrids<sup>[20]</sup>, possessing ribbons of face-sharing octahedra. The exact structure of the hybrids<sup>[8b]</sup> with empirical formula  $(\text{Pyr-C}_4)\text{Pb}_2\text{I}_5$  and  $(\text{CA-C}_4)\text{Pb}_2\text{I}_5$  has not

been determined yet, but it is clear that optically they behave similarly to the literature 1D hybrids.  $(\text{EDBE})\text{PbI}_4$  and  $(4\text{NPEA})_2\text{PbI}_4$  belong to the family of 2D layered (110) perovskites, also called corrugated 2D structures.<sup>[21]</sup> These possess excitonic peaks at lower wavelengths (469 nm and 484 nm, respectively) than the more common 2D layered (100) perovskites. All the hybrids with the excitonic absorption peaks between  $\sim 491$  nm and  $\sim 532$  nm are either confirmed<sup>[8b, 18-19]</sup> (based on single-crystal XRD), or expected<sup>[2b, 4a]</sup> (based on XRD and other optical characteristics) 2D layered (100) perovskites. The excitonic absorption peak position for 2D layered perovskites has been shown to depend mainly on the distortion of the inorganic lattice. With the Pb-I-Pb angle between connected  $\text{PbI}_6^{4-}$  octahedra and the distortion of these octahedra likely being predominant factors influencing the excitonic peak position within the category of 2D layered lead iodide based perovskites.<sup>[7, 19]</sup>

Based on this plot, it can be deduced that the hybrid phases containing the oligothiophenes with an excitonic peak around 440 nm (phase 2) are situated in-between the common 1D hybrids and the 2D layered perovskites in terms of excitonic peak position.

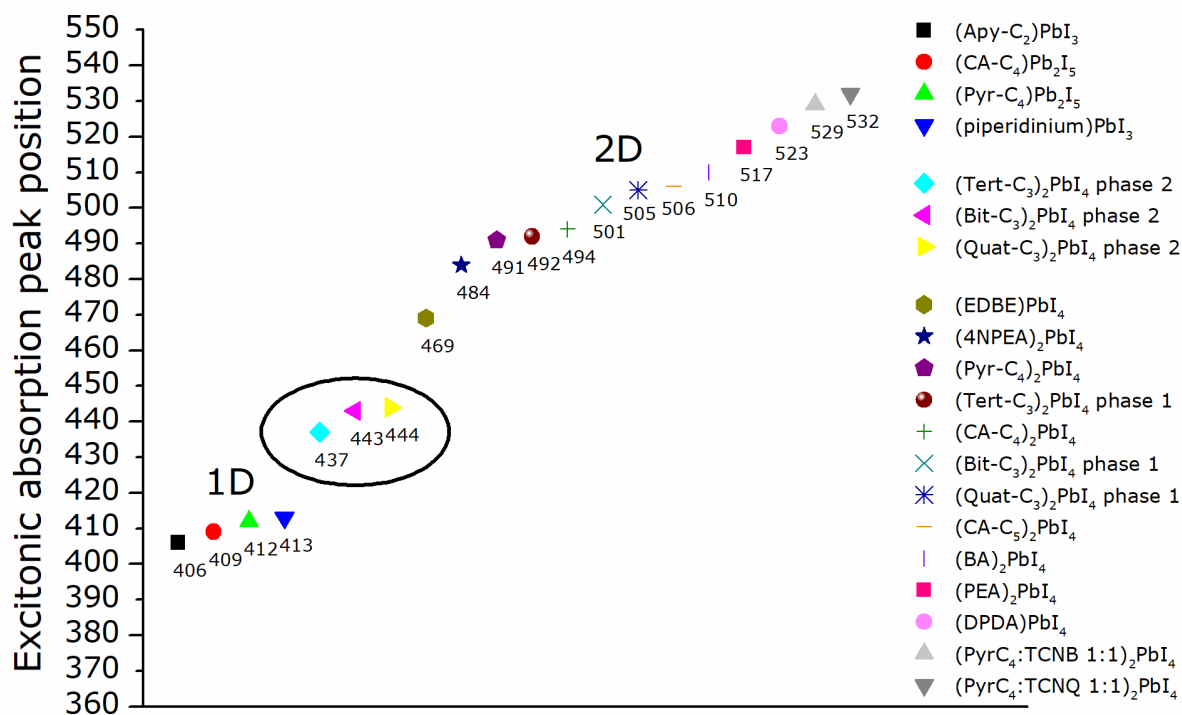


**Figure 10.** Plot with excitonic absorption peak positions for different hybrids. The spacing along the X-axis does not have a physical meaning and was chosen for clarity. The ellipse indicates the excitonic peak positions for phase 2 of the oligothiophene hybrids.  $(\text{Apy-C}_2)\text{PbI}_3$  ( $\text{Apy-C}_2 = 1\text{-ethyl-4-aminopyridinium}$ )<sup>[20a]</sup>,  $(\text{CA-C}_4)_2\text{Pb}_2\text{I}_5$  ( $\text{CA-C}_4 = \text{carbazole-butylammonium}$ )<sup>[8b]</sup>,  $(\text{Pyr-C}_4)\text{Pb}_2\text{I}_5$  ( $\text{Pyr-C}_4 = \text{pyrene-butylammonium}$ )<sup>[8b]</sup>,  $(\text{piper})\text{PbI}_3$  ( $\text{piper} = \text{piperidinium}$ )<sup>[20b]</sup>,  $(\text{Tert-C}_3)_2\text{PbI}_4$  phase 2 ( $\text{Tert-C}_3 = \text{terthiophene-propylammonium}$ ),  $(\text{Bit-C}_3)_2\text{PbI}_4$  phase 2 ( $\text{Bit-C}_3 = \text{bithiophene-propylammonium}$ ),  $(\text{Quat-C}_3)_2\text{PbI}_4$  phase 2 ( $\text{Quat-C}_3 = \text{quaterthiophene-propylammonium}$ ),  $(\text{EDBE})\text{PbI}_4$  ( $\text{EDBE} = 2,2\text{-}(\text{ethylenedioxy})\text{-bis}(\text{ethylammonium})$ )<sup>[21a]</sup>,  $(4\text{NPEA})_2\text{PbI}_4$  ( $4\text{NPEA} = 4\text{-nitrophenylethylammonium}$ )<sup>[21b]</sup>,  $(\text{PyrC}_4)_2\text{PbI}_4$ <sup>[8b]</sup>,  $(\text{Tert-C}_3)_2\text{PbI}_4$  phase 1,  $(\text{CA-C}_4)_2\text{PbI}_4$ <sup>[2b]</sup>,  $(\text{Bit-C}_3)_2\text{PbI}_4$  phase 1,  $(\text{Quat-C}_3)_2\text{PbI}_4$  phase 1,  $(\text{CA-C}_5)_2\text{PbI}_4$  ( $\text{CA-C}_5 = \text{carbazole-pentylammonium}$ ),  $(\text{BA})_2\text{PbI}_4$  ( $\text{BA} = \text{butylammonium}$ )<sup>[18]</sup>,  $(\text{PEA})_2\text{PbI}_4$  ( $\text{PEA} = \text{phenethylammonium}$ )<sup>[19]</sup>,  $(\text{DPDA})\text{PbI}_4$  ( $\text{DPDA} = \text{N,N-dimethylphenylene-p-diammonium}$ )<sup>[19]</sup>,  $(\text{PyrC}_4:\text{TCNB } 1:1)_2\text{PbI}_4$  ( $\text{TCNB} = \text{tetracyanobenzene}$ )<sup>[4a]</sup>,  $(\text{PyrC}_4:\text{TCNQ } 1:1)_2\text{PbI}_4$  ( $\text{TCNQ} = \text{tetracyanoquinodimethane}$ )<sup>[4a]</sup>.

In an attempt to determine the crystal structure of the two phases that are present in the thin films, the growth of single crystals was pursued. Attempts to obtain single crystals from the Quat-C<sub>3</sub>/PbI<sub>2</sub> material system were unsuccessful. However, single crystals suitable for structure elucidation using single-crystal X-ray diffraction of the Tert-C<sub>3</sub>/PbI<sub>2</sub> and Bit-C<sub>3</sub>/PbI<sub>2</sub> material systems were obtained (details on the crystal growth procedures can be found in the supporting information). For the Tert-C<sub>3</sub>/PbI<sub>2</sub> material system, crystals with a chemical formula of (Tert-C<sub>3</sub>)<sub>6</sub>(Pb<sub>2</sub>I<sub>7</sub>)<sub>2</sub>·(H<sub>2</sub>O) were obtained (Figure S29). The inorganic framework contains a combination of corner- and face-sharing octahedra. The structure also contains one water molecule for every six Tert-C<sub>3</sub> molecules. For the Bit-C<sub>3</sub>/PbI<sub>2</sub> material system, similar crystals were obtained with a chemical formula of (Bit-C<sub>3</sub>)<sub>3</sub>Pb<sub>2</sub>I<sub>7</sub>·H<sub>2</sub>O (Figure S30). The inorganic framework also contains a combination of corner- and face-sharing octahedra and there is one water molecule for every three Bit-C<sub>3</sub> molecules. Since the thin films are prepared in a glovebox from precursor solutions containing dry solvents and high annealing temperatures are used, it is highly unlikely that the crystal phases in the thin films contain water molecules. For the Bit-C<sub>3</sub>/PbI<sub>2</sub> material system, also crystals with a chemical formula of (Bit-C<sub>3</sub>)<sub>12</sub>Pb<sub>9</sub>I<sub>30</sub> were obtained (Figure S31). The inorganic framework of these crystals contains a combination of corner- and face-sharing octahedra, but no water molecules are present in the structure. Comparing the simulated pattern of these crystals with the pattern of both phases of Bit-C<sub>3</sub> present in the thin films, it is clear that the pattern of the single crystals does not match with that of either phase (Figure S32). In summary, the crystal phases obtained through single crystal growth do not match with the crystal phases obtained in the thin films. The crystal phase of a hybrid that is obtained through the growth of single crystals is highly dependent on the growth conditions (including the used solvent(s), the concentration of the components, the temperature, the presence of colloids, the pH of the solution and the presence of additives/impurities).<sup>[22]</sup> Understanding the factors that influence the formation of single crystals of these hybrids to consistently obtain a specific (desired) crystal phase goes beyond the scope of the current study and is the topic of future work.

In conclusion, we prepared thin films of hybrids containing quaterthiophene, terthiophene and bithiophene derivatives. We have shown that two different crystal phases can be obtained for these material systems depending on the processing conditions that are used. For the hybrids containing quaterthiophene, it was possible to direct the phase formation completely towards one phase or the other by using either drop-casting or spin-coating. For the terthiophene and bithiophene derivatives, both phases are formed using spin-coating. For the bithiophene derivative, the two phases are obtained together regardless of the annealing temperature that is used. Through a comparison with established 2D and 1D hybrids, we have shown that one of the phases that can be obtained using these oligothiophenes possesses a (electronic) dimensionality intermediate between 2D and 1D.

## Author contributions

The manuscript was written through contributions of all authors. W.T.M.V.G. and R.H. contributed equally to this work, as shared first authors.† All authors have given approval to the final version of the manuscript.

## Acknowledgements

The FWO is acknowledged for the funding of the research. P-H.D. is a special research fund (BOF) doctoral (Ph.D.) student at UHasselt/IMO, and M.M. is an SB Ph.D. fellow at FWO (Number 1S20118N). W.T.M.V.G., L.L., and D.V. acknowledge the FWO for the funding of the SBO project PROCEED (FWO-S002019N) and the senior FWO research project G043320N. K.V.H. thanks the Research Foundation – Flanders (FWO) (projects AUGÉ/11/029 and G099319N) for funding. The work has been carried out in the context of the Solliance network ([www.solliance.eu](http://www.solliance.eu)), from which UHasselt is a member. Additionally, UHasselt is a partner in the Energyville Consortium (<http://www.energyville.be/about-energyville>).

**Keywords:** low-dimensional • organic-inorganic hybrid composites • perovskite phases • stability • oligothiophenes

- [1] a) L. Mao, C. C. Stoumpos, M. G. Kanatzidis, *J Am Chem Soc* **2019**, *141*, 1171-1190; b) G. Grancini, M. K. Nazeeruddin, *Nat Rev Mater* **2018**, *4*, 4-22; c) C. Ortiz-Cervantes, P. Carmona-Monroy, D. Solis-Ibarra, *ChemSusChem* **2019**, *12*, 1560-1575; d) H. Lin, C. Zhou, Y. Tian, T. Siegrist, B. Ma, *ACS Energy Letters* **2017**, *3*, 54-62.
- [2] a) A. Krishna, S. Gottis, M. K. Nazeeruddin, F. Sauvage, *Advanced Functional Materials* **2019**, *29*; b) R. Herckens, W. T. M. Van Gompel, W. Y. Song, M. C. Gelvez-Rueda, A. Maufort, B. Ruttens, J. D'Haen, F. C. Grozema, T. Aernouts, L. Lutsen, D. Vanderzande, *Journal of Materials Chemistry A* **2018**, *6*, 22899-22908.
- [3] a) B. Saparov, D. B. Mitzi, *Chem Rev* **2016**, *116*, 4558-4596; b) M. I. Saidaminov, O. F. Mohammed, O. M. Bakr, *Acs Energy Letters* **2017**, *2*, 889-896.
- [4] a) W. T. M. Van Gompel, R. Herckens, K. Van Hecke, B. Ruttens, J. D'Haen, L. Lutsen, D. Vanderzande, *Chem Commun (Camb)* **2019**, *55*, 2481-2484; b) A. C. Veron, A. Linden, N. A. Leclaire, E. Roedern, S. Hu, W. Ren, D. Rentsch, F. A. Nuesch, *J Phys Chem Lett* **2018**, *9*, 2438-2442; c) X. Li, J. Yang, Z. Song, R. Chen, L. Ma, H. Li, J. Jia, J. Meng, X. Li, M. Yi, X. Sun, *ACS Applied Energy Materials* **2018**, *1*, 4467-4472.
- [5] a) H. Hu, F. Meier, D. Zhao, Y. Abe, Y. Gao, B. Chen, T. Salim, E. E. M. Chia, X. Qiao, C. Deibel, Y. M. Lam, *Adv Mater* **2018**, *30*, e1707621; b) M. D. Smith, B. A. Connor, H. I. Karunadasa, *Chem Rev* **2019**, *119*, 3104-3139; c) K. Jemli, P. Audebert, L. Galmiche, G. Trippe-Allard, D. Garrot, J. S. Lauret, E. Deleporte, *ACS Appl Mater Interfaces* **2015**, *7*, 21763-21769; d) M. Braun, W. Tuffentsammer, H. Wachtel, H. C. Wolf, *Chemical Physics Letters* **1999**, *303*, 157-164.

- [6] a) C. Ortiz-Cervantes, P. I. Roman-Roman, J. Vazquez-Chavez, M. Hernandez-Rodriguez, D. Solis-Ibarra, *Angew Chem Int Ed Engl* **2018**, *57*, 13882-13886; b) J. V. Passarelli, D. J. Fairfield, N. A. Sather, M. P. Hendricks, H. Sai, C. L. Stern, S. I. Stupp, *J Am Chem Soc* **2018**, *140*, 7313-7323; c) M. C. Gelvez-Rueda, W. T. M. Van Gompel, R. Herckens, L. Lutsen, D. Vanderzande, F. C. Grozema, *J Phys Chem Lett* **2020**, *11*, 824-830; d) N. Marchal, W. Van Gompel, M. C. Gelvez-Rueda, K. Vandewal, K. Van Hecke, H. G. Boyen, B. Conings, R. Herckens, S. Maheshwar, L. Lutsen, C. Quarti, F. C. Grozema, D. Vanderzande, D. Beljonne, *Chemistry of Materials* **2019**, *31*, 6880-6888.
- [7] K. Z. Du, Q. Tu, X. Zhang, Q. Han, J. Liu, S. Zauscher, D. B. Mitzi, *Inorg Chem* **2017**, *56*, 9291-9302.
- [8] a) C. J. Que, C. J. Mo, Z. Q. Li, G. L. Zhang, Q. Y. Zhu, J. Dai, *Inorg Chem* **2017**, *56*, 2467-2472; b) W. T. M. Van Gompel, R. Herckens, K. Van Hecke, B. Ruttens, J. D'Haen, L. Lutsen, D. Vanderzande, *ChemNanoMat* **2019**, *5*, 323-327; c) W. T. M. Van Gompel, R. Herckens, P.-H. Denis, M. Mertens, M. C. Gelvez-Rueda, K. Van Hecke, B. Ruttens, J. D'Haen, F. C. Grozema, L. Lutsen, D. Vanderzande, *Journal of Materials Chemistry C* **2020**, *8*, 7181-7188.
- [9] a) Z. W. Xiao, W. W. Meng, J. B. Wang, D. B. Mitzi, Y. F. Yan, *Materials Horizons* **2017**, *4*, 206-216; b) J. M. Hoffman, X. Che, S. Sidhik, X. Li, I. Hadar, J. C. Blancon, H. Yamaguchi, M. Kepenekian, C. Katan, J. Even, C. C. Stoumpos, A. D. Mohite, M. G. Kanatzidis, *J Am Chem Soc* **2019**, *141*, 10661-10676.
- [10] a) J. Y. Qian, Q. Guo, L. J. Liu, B. Xu, W. J. Tian, *Journal of Materials Chemistry A* **2017**, *5*, 16786-16795; b) C. Katan, N. Mercier, J. Even, *Chem Rev* **2019**, *119*, 3140-3192.
- [11] M. E. Kamminga, G. A. de Wijs, R. W. A. Havenith, G. R. Blake, T. T. M. Palstra, *Inorg Chem* **2017**, *56*, 8408-8414.
- [12] a) J. Roncali, P. Leriche, P. Blanchard, *Adv Mater* **2014**, *26*, 3821-3838; b) A. Mishra, C. Q. Ma, P. Bauerle, *Chem Rev* **2009**, *109*, 1141-1276.
- [13] a) D. B. Mitzi, K. Chondroudis, C. R. Kagan, *Inorg Chem* **1999**, *38*, 6246-6256; b) K. Chondroudis, D. B. Mitzi, *Chemistry of Materials* **1999**, *11*, 3028-3030.
- [14] X. H. Zhu, N. Mercier, P. Frere, P. Blanchard, J. Roncali, M. Allain, C. Pasquier, A. Riou, *Inorg Chem* **2003**, *42*, 5330-5339.
- [15] a) C. Liu, W. Huhn, K. Z. Du, A. Vazquez-Mayagoitia, D. Dirkes, W. You, Y. Kanai, D. B. Mitzi, V. Blum, *Phys Rev Lett* **2018**, *121*, 146401; b) W. A. Dunlap-Shohl, E. T. Barraza, A. Barrette, S. Dovletgeldi, G. Findik, D. J. Dirkes, C. Liu, M. K. Jana, V. Blum, W. You, K. Gundogdu, A. D. Stiff-Roberts, D. B. Mitzi, *Materials Horizons* **2019**, *6*, 1707-1716; c) Y. Gao, E. Shi, S. Deng, S. B. Shiring, J. M. Snaider, C. Liang, B. Yuan, R. Song, S. M. Janke, A. Liebman-Pelaez, P. Yoo, M. Zeller, B. W. Boudouris, P. Liao, C. Zhu, V. Blum, Y. Yu, B. M. Savoie, L. Huang, L. Dou, *Nat Chem* **2019**, *11*, 1151-1157; d) S. Deng, J. M. Snaider, Y. Gao, E. Shi, L. Jin, R. D. Schaller, L. Dou, L. Huang, *J Chem Phys* **2020**, *152*, 044711; e) E. Shi, B. Yuan, S. B. Shiring, Y. Gao, Akriti, Y. Guo, C. Su, M. Lai, P. Yang, J. Kong, B. M. Savoie, Y. Yu, L. Dou, *Nature* **2020**, *580*, 614-620.
- [16] a) D. H. Cao, C. C. Stoumpos, O. K. Farha, J. T. Hupp, M. G. Kanatzidis, *J Am Chem Soc* **2015**, *137*, 7843-7850; b) X. Y. Gan, O. Wang, K. Y. Liu, X. J. Du, L. L. Guo, H. X. Liu, *Solar Energy Materials and Solar Cells* **2017**, *162*, 93-102.
- [17] Z. N. Song, S. C. Watthage, A. B. Phillips, B. L. Tompkins, R. J. Ellingson, M. J. Heben, *Chemistry of Materials* **2015**, *27*, 4612-4619.
- [18] E. Amerling, S. Baniya, E. Lafalce, C. Zhang, Z. V. Vardeny, L. Whittaker-Brooks, *J Phys Chem Lett* **2017**, *8*, 4557-4564.
- [19] M. P. Hautzinger, J. Dai, Y. Ji, Y. Fu, J. Chen, I. A. Guzei, J. C. Wright, Y. Li, S. Jin, *Inorg Chem* **2017**, *56*, 14991-14998.
- [20] a) H. B. Duan, S. S. Yu, S. X. Liu, H. Zhang, *Dalton Trans* **2017**, *46*, 2220-2227; b) G. C. Papavassiliou, I. B. Koutselas, *Synthetic Metals* **1995**, *71*, 1713-1714.
- [21] a) D. Cortecchia, S. Neutzner, A. R. Srimath Kandada, E. Mosconi, D. Meggiolaro, F. De Angelis, C. Soci, A. Petrozza, *J Am Chem Soc* **2017**, *139*, 39-42; b) M. H. Tremblay, F. Thouin, J. Leisen, J. Bacsa, A. R. Srimath Kandada, J. M. Hoffman, M. G. Kanatzidis, A. D. Mohite, C. Silva, S. Barlow, S. R. Marder, *J Am Chem Soc* **2019**, *141*, 4521-4525.
- [22] a) L. Ke, S. Luo, X. Ren, Y. Yuan, *Journal of Physics D: Applied Physics* **2021**, *54*, 163001; b) P. K. Nayak, D. T. Moore, B. Wenger, S. Nayak, A. A. Haghighirad, A. Fineberg, N. K. Noel, O. G. Reid, G. Rumbles, P. Kukura, K. A. Vincent, H. J. Snaith, *Nat Commun* **2016**, *7*, 13303; c) K. Yan, M. Long, T. Zhang, Z. Wei, H. Chen, S. Yang, J. Xu, *J Am Chem Soc* **2015**, *137*, 4460-4468.